

# We are IntechOpen, the world's leading publisher of Open Access books Built by scientists, for scientists

6,900

Open access books available

186,000

International authors and editors

200M

Downloads

Our authors are among the

154

Countries delivered to

TOP 1%

most cited scientists

12.2%

Contributors from top 500 universities



WEB OF SCIENCE™

Selection of our books indexed in the Book Citation Index  
in Web of Science™ Core Collection (BKCI)

Interested in publishing with us?  
Contact [book.department@intechopen.com](mailto:book.department@intechopen.com)

Numbers displayed above are based on latest data collected.  
For more information visit [www.intechopen.com](http://www.intechopen.com)



# Discrete Wavelet Transform for Nonstationary Signal Processing

Yansong Wang, Weiwei Wu, Qiang Zhu and Gongqi Shen  
*Shanghai University of Engineering Science,  
P. R. China*

## 1. Introduction

In engineering, digital signal processing techniques need to be carefully selected according to the characteristics of the signals of interest. The frequency-based and time-frequency techniques have been frequently mentioned in some literature (Cohen, 1995). The frequency-based techniques (FBTs) have been widely used for stationary signal analysis. For nonstationary signals, the time-frequency techniques (TFTs) in common use, such as short-time Fourier transform (STFT), wavelet transform (WT), ambiguity function (AF) and wigner-ville distribution (WVD), etc., are usually performed for extracting transient features of the signals. These techniques use different algorithms to produce a time-frequency representation for a signal.

The STFT uses a standard Fourier transform over several types of windows. Wavelet-based techniques apply a mother wavelet with either discrete or continuous scales to a waveform to resolve the fixed time-frequency resolution issues inherent in STFT. In applications, the fast version of wavelet transform, that is attributed to a pair of mirror filters with variable sampling rates, is usually used for reducing the number of calculations to be done, thereby saving computer running time. AF and WVD are quadratic time-frequency representations, that use advanced techniques to combat these resolution difficulties. They have better resolution than STFT but suffer from cross-term interference and produce results with coarser granularity than wavelet techniques do. Of the wavelet-based techniques, discrete wavelet transform (DWT), especially its fast version, is usually used for encoding and decoding signals, while wavelet packet analysis (WPA) are successful in signal recognition and characteristic extraction. AF and WVD with excessive transformation durations are obviously unacceptable in the development of real-time monitoring systems.

In applications, the FBTs were typically used in noise and vibration engineering (Brigham, 1988). They provide the time-averaged energy information from a signal segment in frequency domain, but remain nothing in time domain. For nonstationary signals such as vehicle noises, some implementation examples are the STFT (Hodges & Power, 1985), WVD, smoothed pseudo-WVD (Baydar & Ball, 2001) and WT (Chen, 1998). In particular, the WT as “mathematical microscope” in engineering allows the changing spectral composition of a nonstationary signal to be measured and presented in the form of a time-frequency map and thus, was suggested as an effective tool for nonstationary signal analysis.

This chapter includes three sections. We firstly briefly introduce the theory background of the Wavelet-based techniques, such as the CWT, DWT, WPA, as well as the Mallat filtering scheme and algorithm for the DWT-based calculation. Secondly, we discuss the advantages and drawbacks of the DWT-based methods in nonstationary signal processing by comparing the DWT with other TFTs. Some successful examples of the DWT used for nonstationary vibration and sound signals in the vehicle engineering will be given in the third section.

## 2. Theory background

### 2.1 Continuous wavelet transform

For a function or signal  $x(t) \in L^2(R)$ , if a prototype or mother wavelet is given as  $\psi(t)$ , then the wavelet transform can be expressed as:

$$\text{CWT}_x(a, b) = \frac{1}{\sqrt{a}} \int x(t) \overline{\psi\left(\frac{t-b}{a}\right)} dt = \langle x(t), \psi_{ab}(t) \rangle \quad (1)$$

Here  $a$  and  $b$  change continuously, so comes the name continuous wavelet transform (CWT). A family of wavelets  $\psi_{ab}(t)$ , each of which can be seen as a filter, is defined in (1) by dilating and translating of  $\psi(t)$ . Obviously,  $b$  changes along the time axle, its role is simple and clear. Variable  $a$  acts as a scale function, its change alters not only the spectrum of the wavelet function, but also the size of its time-frequency window. The local information in time and frequency domain, which reflects different characteristics of the signal, is extracted by CWT.

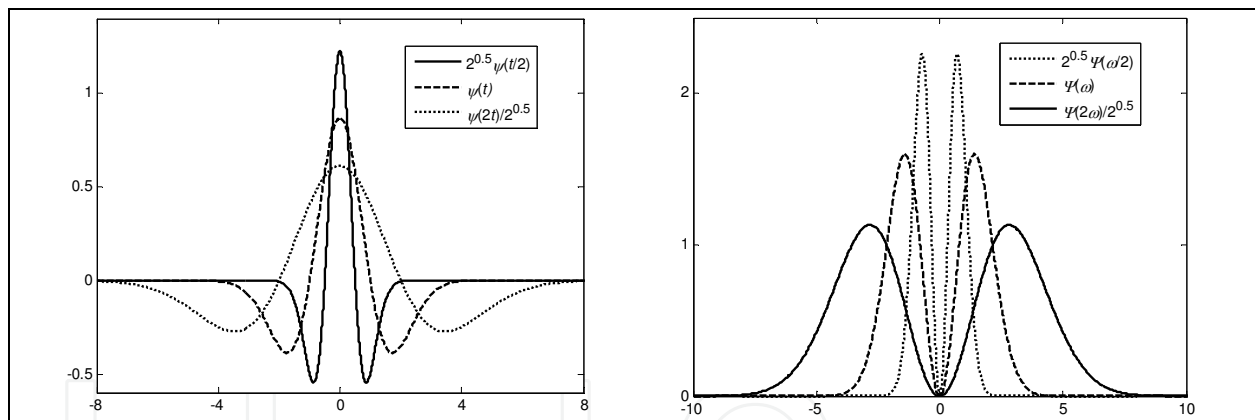


Fig. 1. "mexico hat" wavelets with different  $a$  and their spectra

If  $c_\psi = \int \frac{|\Psi(\omega)|^2}{\omega} d\omega < \infty$  is satisfied, where  $\Psi(\omega)$  is the Fourier transform of  $\psi(t)$ , then  $\psi(t)$  is an admissible wavelet. In this condition, original signal  $x(t)$  can be recovered from its CWT by:

$$x(t) = \frac{1}{c_\psi} \iint \text{CWT}_x(a, b) \psi_{ab}(t) \frac{da db}{a^2} \quad (2)$$

In the case where  $\psi$  is also  $L^1(R)$ , the admissibility condition implies that  $\Psi(0)=0$ ;  $\psi$  has mean value 0, is oscillating, and decays to zero at infinity; these properties explain the qualification as "wavelet" of this function  $\psi(t)$ . From the view of signal processing,  $\psi(t)$  acts as a band pass filter.

## 2.2 Discrete wavelet transform

The time-frequency windows of  $\psi_{ab}(t)$  are overlapped each other, which means there is information redundancy in CWT. This is a disadvantage of CWT when it is used for signal compression or feature extraction. Thus the wavelet transform can be computed discretely on the time-frequency plane, to reduce the redundancy. The crucial point is how to sample  $a$  and  $b$  to guarantee the precise reconstruction of original signal  $x(t)$  from its wavelet transform. There are several forms of wavelet transform according to the different level of discretization.

Simply let  $a = a_0^j$ , where  $a_0 > 0$  and  $j \in \mathbb{Z}$ , we can discretize  $a$ . Generally we have  $a_0 = 2$ , thus the scale is sampled along a dyadic sequence, so the function  $\psi_{jb}(t) = \frac{1}{\sqrt{2^j}} \psi\left(\frac{t-b}{2^j}\right)$  is a dyadic wavelet, and the corresponding transform  $WT_x(j, b) = \frac{1}{\sqrt{2^j}} \int x(t) \psi\left(\frac{t-b}{2^j}\right) dt = \langle x(t), \psi_{jb}(t) \rangle$  is called dyadic wavelet transform.

To recover  $x(t)$  from its dyadic wavelet transform, the dual wavelet  $\hat{\psi}(t)$  of  $\psi(t)$  must be introduced. Dual wavelet has the same scale and time shift as original wavelet, that is  $\hat{\psi}_{jb}(t) = \frac{1}{\sqrt{2^j}} \hat{\psi}\left(\frac{t-b}{2^j}\right)$ . The relationship between  $\hat{\psi}(t)$  and  $\psi(t)$  is:  $\hat{\Psi}(\omega) = \frac{\Psi(\omega)}{\sum_{j=-\infty}^{\infty} |\Psi(2^j \omega)|^2}$ ,

where  $\hat{\Psi}(\omega)$  is the Fourier transform of  $\hat{\psi}(t)$ . We can prove  $x(t)$  is reconstructed by:

$$x(t) = \sum_{j=-\infty}^{\infty} 2^{-3j/2} \int WT_x(j, b) \hat{\psi}\left(\frac{t-b}{2^j}\right) db \quad (3)$$

To ensure the recovery, there should be  $A \leq \sum_{j=-\infty}^{\infty} |\Psi(2^j \omega)|^2 \leq B$ , where  $A$  and  $B$  are constants,

this is the stability condition. Obviously, dual wavelet of a stable function is also stable.

To step further, we sample time domain by taking  $b = kb_0$ , where  $b_0$  should be chosen to ensure the recovery of  $x(t)$ . When  $a$  is changed from  $a_0^{j-1}$  to  $a_0^j$ , the central frequency and the band width of the wavelet are all decreased by  $a_0$  times, so the sample interval can increase to  $a_0$  times. In this case, the discretized wavelet function is  $\psi_{jk}(t) = \frac{1}{\sqrt{a_0^j}} \psi\left(\frac{t - ka_0^j b_0}{a_0^j}\right)$ , and its

wavelet transform is:  $WT_x(j, k) = \frac{1}{\sqrt{a_0^j}} \int x(t) \psi\left(\frac{t - ka_0^j b_0}{a_0^j}\right) dt = \langle x(t), \psi_{jk}(t) \rangle$ . This decomposition

is called discrete wavelet transform (DWT). From this formula, while time  $t$  is still continuous, we only compute the wavelet transform on a grid in the time-frequency plane, as depicted in Fig. 2.

Given  $d_j(k) = WT_x(j, k)$ , we hope to recover  $x(t)$  from formula like

$$x(t) = \sum_{j=0}^{\infty} \sum_{k=-\infty}^{\infty} d_j(k) \hat{\psi}_{jk}(t) \quad (4)$$

This formula is called wavelet series, in which  $d_j(k)$  is wavelet coefficients and  $\hat{\psi}_{jk}(t)$  is dual wavelet. To recover  $x(t)$  using (4), many questions should be answered, such as: are  $\psi_{jk}(t)$  complete to describe arbitrary signal  $x(t) \in L^2(R)$ ; is there information redundancy in the decomposition; how to determine the sample interval of  $a$  and  $b$ . Daubechies studied them thoroughly, and her wavelet frame theory answered these questions [1].

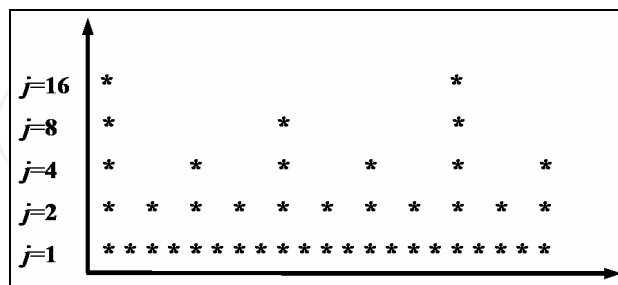


Fig. 2. The computing grid of DWT

We call a function family  $\{\psi_n\}$  a frame if there exist two constants  $A>0$  and  $B>0$  such that for an arbitrary  $x(t) \in L^2(R)$ ,  $A\|x\|^2 \leq \sum_n |\langle x, \psi_n \rangle|^2 \leq B\|x\|^2$  is satisfied. When  $A=B$  the frame is said to

be tight. A frame defines a complete and stable signal representation, which may also be redundant. When the frame vectors are normalized  $\|\psi_n\|^2 = 1$ , the redundancy is measured by the frame bounds  $A$  and  $B$ . The frame is an orthogonal basis if and only if  $A=B=1$ . If  $A>1$  then the frame is redundant and  $A$  can be interpreted as a minimum redundancy factor.

If a frame operator  $S$  is defined as  $Sx = \sum_n \langle x, \psi_n \rangle \psi_n$ , then  $x = \sum_n \langle x, S^{-1}\psi_n \rangle \psi_n = \sum_n \langle x, \psi_n \rangle S^{-1}\psi_n$ ,

so we can define  $\hat{\psi}_n = S^{-1}\psi_n$  as the dual frame of  $\psi_n$ , with bounds  $A^{-1}$  and  $B^{-1}$ . If  $A=B$ , we have  $\hat{\psi}_n = \frac{1}{A}\psi_n$ . So the recovery process in (4) is well founded. In many cases where precise

reconstruction is not a pursuit, we can take  $\hat{\psi}_{jk}(t) \approx \frac{2}{A+B}\psi_{jk}(t)$ ,

$$x(t) = \frac{2}{A+B} \sum_{j,k} \langle x(t), \psi_{jk}(t) \rangle \psi_{jk}(t) + e(t), \text{ here } e(t) \text{ is the error and } \|e(t)\| \leq \frac{B-A}{B+A} \|f\|.$$

The only remain problem is how to construct a wavelet frame. Obviously, the smaller  $b_0$  and  $a_0$  are, the greater the information redundancy is, and the reconstruction is easier. On the contrary,  $\psi_n$  will be incomplete when  $b_0$  and  $a_0$  are big enough, which make precise recovery

of  $x(t)$  impossible. For this problem, there are two theorems: (1) If  $\psi_{jk}(t) = a_0^{-\frac{j}{2}} \psi(a_0^{-j}t - kb_0)$

is a frame of  $L^2(R)$  then the frame bounds satisfy  $A \leq \frac{2\pi \int_0^\infty \frac{|\Psi(\omega)|^2}{\omega} d\omega}{b_0 \ln a_0} \leq B$ ; (2) Define

$$\beta(\xi) = \sup_{0 \leq |\omega| \leq a_0} \sum_{j=-\infty}^\infty |\Psi(a_0^j \omega)| |\Psi(a_0^j \omega + \xi)| \text{ and } \Delta = \sum_{\substack{k=-\infty \\ k \neq 0}}^\infty [\beta(\frac{2\pi k}{b_0}) \beta(\frac{-2\pi k}{b_0})]^{\frac{1}{2}}, \text{ if } b_0 \text{ and } a_0 \text{ are such that}$$

$$A_0 = \frac{1}{b_0} \left( \inf_{0 \leq |\omega| \leq a_0} \sum_{j=-\infty}^{\infty} |\Psi(a_0^j \omega)|^2 - \Delta \right) > 0 \text{ and } B_0 = \frac{1}{b_0} \left( \inf_{0 \leq |\omega| \leq a_0} \sum_{j=-\infty}^{\infty} |\Psi(a_0^j \omega)|^2 + \Delta \right) < \infty, \text{ then } \{\psi_{jk}(t)\} \text{ is}$$

a frame of  $L^2(\mathbb{R})$ . These two theorems are the sufficient and necessary conditions to construct wavelet frame.

In some cases, wavelet frame  $\{\psi_{jk}(t)\}$  is orthogonal or independent, the more correlated the functions are, the smaller the subspace spanned by the frame is. This is useful in noise reduction. When  $b_0$  and  $a_0$  is close to 0 and 1, the functions of the frame are strongly related and behave like continuous wavelet. In other cases, redundancy or dependency is avoided as possible, so  $\psi$ ,  $b_0$  and  $a_0$  are chosen to compose an orthogonal basis.

### 2.3 Multiresolution analysis and mallat algorithm

Multiresolution analyze (MRA) provides an elegant way to construct wavelet with different properties. A sequence  $\{V_j\}_{j \in \mathbb{Z}}$  of closed subspaces of  $L^2(\mathbb{R})$  is a MRA if the following 6 properties are satisfied:

1.  $\forall (j, k) \in \mathbb{Z}, f(t) \in V_j \Leftrightarrow f(t - 2^j k) \in V_j,$
2.  $\forall j \in \mathbb{Z}, V_{j+1} \subset V_j,$
3.  $\forall j \in \mathbb{Z}, f(t) \in V_j \Leftrightarrow f(\frac{t}{2}) \in V_{j+1},$
4.  $\lim_{j \rightarrow \infty} V_j = \bigcap_{j=-\infty}^{\infty} V_j = \{0\},$
5.  $\lim_{j \rightarrow -\infty} V_j = \text{Closure}(\bigcup_{j=-\infty}^{\infty} V_j) = L^2(\mathbb{R}),$
6. There exists  $\theta$  such that  $\{\theta(t-n)\}_{n \in \mathbb{Z}}$  is a Riesz basis of  $V_0$ .

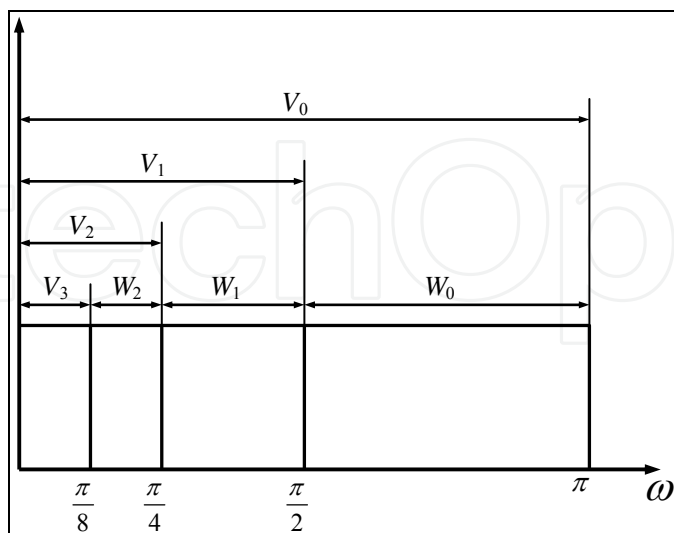


Fig. 3. Partition of function space by multiresolution analyze

The main idea of MRA is described in Fig. 3, the space  $L^2(\mathbb{R})$  is orderly partitioned. The relationship between adjacent spaces  $V_j$  and  $V_{j+1}$  is reflected from condition 2) and 3), so the

basis of  $V_j$  and  $V_{j+1}$  differs only on the scale by 2. We only discuss how to construct an orthogonal wavelet basis here, so a space series  $W_j$  which satisfy  $V_j \oplus W_j \subset V_{j-1}$  are introduced. By this idea, the function space can be decomposed like

$$V_0 = W_1 \oplus W_2 \oplus \dots \oplus W_j \oplus V_j \text{ and so } L^2(\mathbb{R}) = \bigoplus_{m=-\infty}^{\infty} W_m, \text{ which can be seen in Fig. 3.}$$

By this kind of decomposition, components in each space  $W_j$  contain different details of the function, or from the view of signal processing, the original signal is decomposed by a group of orthogonal filters.

To construct an orthogonal wavelet basis, we first need to find an orthogonal basis of  $V_0$ . From the following theorem: a family  $\{\varphi(t-n)\}_{n \in \mathbb{Z}}$  is a standard orthogonal basis  $\leftrightarrow$

$$\sum_{k \in \mathbb{Z}} |\Phi(\omega + 2k\pi)|^2 = 1, \text{ where } \Phi(\omega) \text{ is the Fourier transform of } \varphi(t). \text{ If } \{\theta(t-n)\}_{n \in \mathbb{Z}}, \text{ with Fourier}$$

transform  $\Theta(\omega)$ , is not an orthogonal basis of  $V_0$ , from the above theorem, we can compute

$$\Phi(\omega) = \frac{\Theta(\omega)}{\sum_{k \in \mathbb{Z}} |\Theta(\omega + 2k\pi)|^2}, \text{ and } \{\varphi(t-n)\}_{n \in \mathbb{Z}} \text{ must be orthogonal. We call } \varphi(t) \text{ the scale function,}$$

and we will take  $\{\varphi(t-n)\}_{n \in \mathbb{Z}}$  as the orthogonal basis of  $V_0$  in this chapter.

From above discussion,  $\{\varphi(t-n)\}_{n \in \mathbb{Z}}$  is an orthogonal basis of  $V_0$ , and  $\varphi(\frac{t}{2}) \in V_1 \subset V_0$ , we have

$$\varphi(\frac{t}{2}) = \sqrt{2} \sum_{k=-\infty}^{\infty} h(k)\varphi(t-k). \text{ In the frequency, } \sqrt{2}\Phi(2\omega) = H(\omega)\Phi(\omega), \text{ where}$$

$$H(\omega) = \sum_{k=-\infty}^{\infty} h(k)e^{-ik\omega}. \text{ If we take } \{\psi(\frac{t}{2}-n)\}_{n \in \mathbb{Z}} \text{ as an orthogonal basis of } W_1, \text{ since we have}$$

$$V_0 = V_1 \oplus W_1 \text{ from above discussion of MRA, then } \psi(\frac{t}{2}) = \sqrt{2} \sum_{k=-\infty}^{\infty} g(k)\varphi(t-k) \text{ and}$$

$$\sqrt{2}\Psi(2\omega) = G(\omega)\Phi(\omega) \text{ are hold. Combine all these expressions with } \int \psi(t)dt = 0 \text{ and}$$

$$\int \varphi(t)dt = 1, \text{ we have following conclusions: 1) } \sum_k h(k) = \sqrt{2} \text{ and } \sum_k g(k) = 0; 2) H(0) = \sqrt{2}$$

and  $G(0)=0$ . From this,  $H$  is a low pass filter and  $G$  band pass filter.

From formula  $\sum_{k \in \mathbb{Z}} |\Phi(\omega + 2k\pi)|^2 = 1$ , which means  $\{\varphi(t-n)\}_{n \in \mathbb{Z}}$  is an orthogonal basis, we have

$$|H(\omega)|^2 + |H(\omega + \pi)|^2 = 2 \tag{5}$$

hold for arbitrary  $\omega$ . The same conclusion is hold for  $G$ , that is

$$|G(\omega)|^2 + |G(\omega + \pi)|^2 = 2 \tag{6}$$

Since the orthogonality between  $\{\varphi(t-n)\}_{n \in \mathbb{Z}}$  and  $\{\psi(t-n)\}_{n \in \mathbb{Z}}$ ,

$$H(\omega)\overline{G(\omega)} + H(\omega + \pi)\overline{G(\omega + \pi)} = 0 \tag{7}$$

must be satisfied. One solution of (7) is  $G(\omega) = -e^{-i\omega} \overline{H(\omega + \pi)}$ , or equivalently  $g(k) = (-1)^k h(1-k)$ . Till here, the constructive method of an orthogonal wavelet basis is completed.

From MRA, Mallat developed a fast algorithm to compute DWT of a given signal. Suppose  $x_{j-1}(k)$ ,  $x_j(k)$  and  $d_j(k)$  are coefficients of  $x(t)$  projected on  $V_{j-1}$ ,  $V_j$  and  $W_j$ ,  $d_j(k)$  here has the same meaning with that in (4), which is  $WT_x(j,k)$ . The Mallat algorithm includes the following Eqs:

$$x_j(k) = \sum_{n=-\infty}^{\infty} x_{j-1}(n)h(n-2k) = x_{j-1}(k) * h(2k) \tag{8}$$

$$d_j(k) = \sum_{n=-\infty}^{\infty} x_{j-1}(n)g(n-2k) = x_{j-1}(k) * g(2k) \tag{9}$$

$$x_{j-1}(k) = \sum_{n=-\infty}^{\infty} x_j(n)h(k-2n) + \sum_{n=-\infty}^{\infty} d_j(n)g(k-2n) \tag{10}$$

In them, (8) and (9) are for decomposition and (10) is for reconstruction. By decomposing it recursively, as in Fig. 4(a), the approximate signal  $x_j(k)$  and detail signal  $d_j(k)$  are computed out successively.

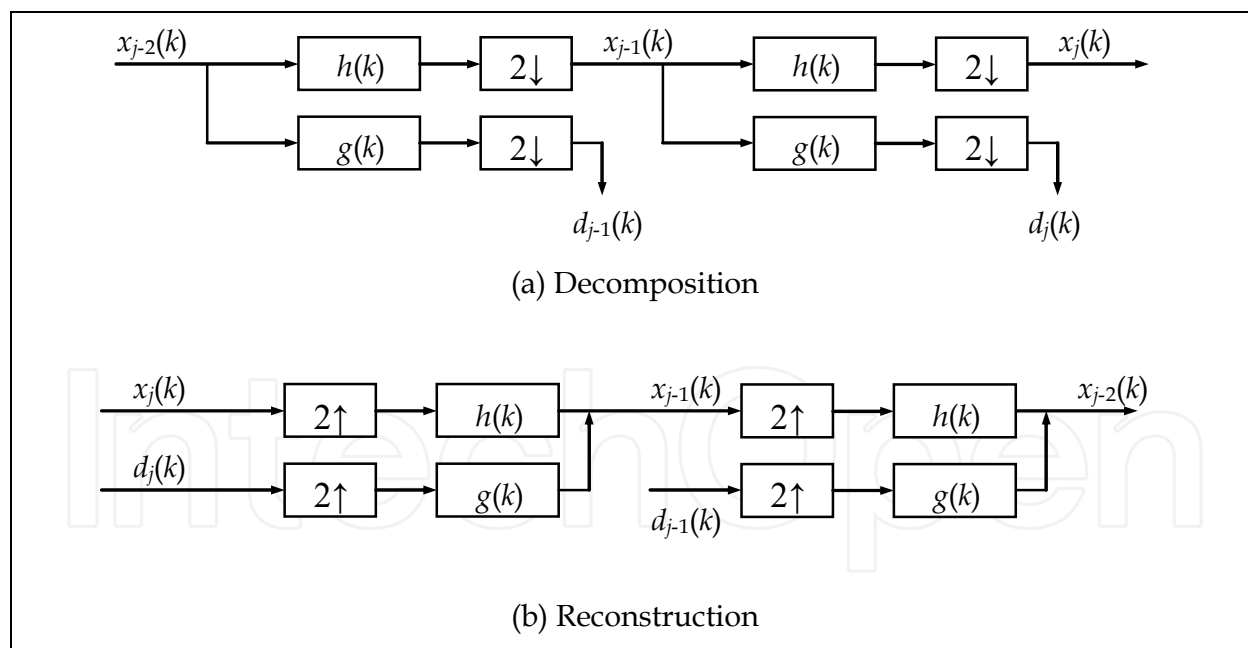


Fig. 4. The Mallat algorithm

### 3. Time-frequency representation comparisons

The task of signal processing is to find the traits of the signals of interest. As known that most of the signals in engineering are obtained in time domain. However, features of the signals can usually be interpreted in frequency domain, so the frequency domain analysis is

important in signal analysis. The Fourier transform and its inversion connect the frequency domain features with the time domain features. Their definitions are as below:

$$X(f) = \int x(t)e^{-j2\pi ft} dt \quad (11)$$

$$x(t) = \int X(f)e^{j2\pi ft} df \quad (12)$$

In the stationary signal analysis, one may use the Fourier transform and its inversion to establish the mapping relation between the time and frequency domains. However, in the practical applications, the Fourier transform is not the best tool for signal analysis due to the nonstationary and time varying feature in the most engineering signals, such as engine vibration and noise signals. For these signals, although their frequency elements can be observed from their frequency spectrum, the time of frequency occurrence and frequency change relationship over time can not be acquired. For further research on these signals, the time-frequency descriptions are introduced. Fig. 5 shows three time-frequency descriptions of the linear frequency modulation signal generated from the Matlab Toolbox: (a) is the frequency domain description which loses the time information; (c) is the time domain description which loses the frequency information; (b) is the time-frequency description which shows the change rule of frequency over time clearly.

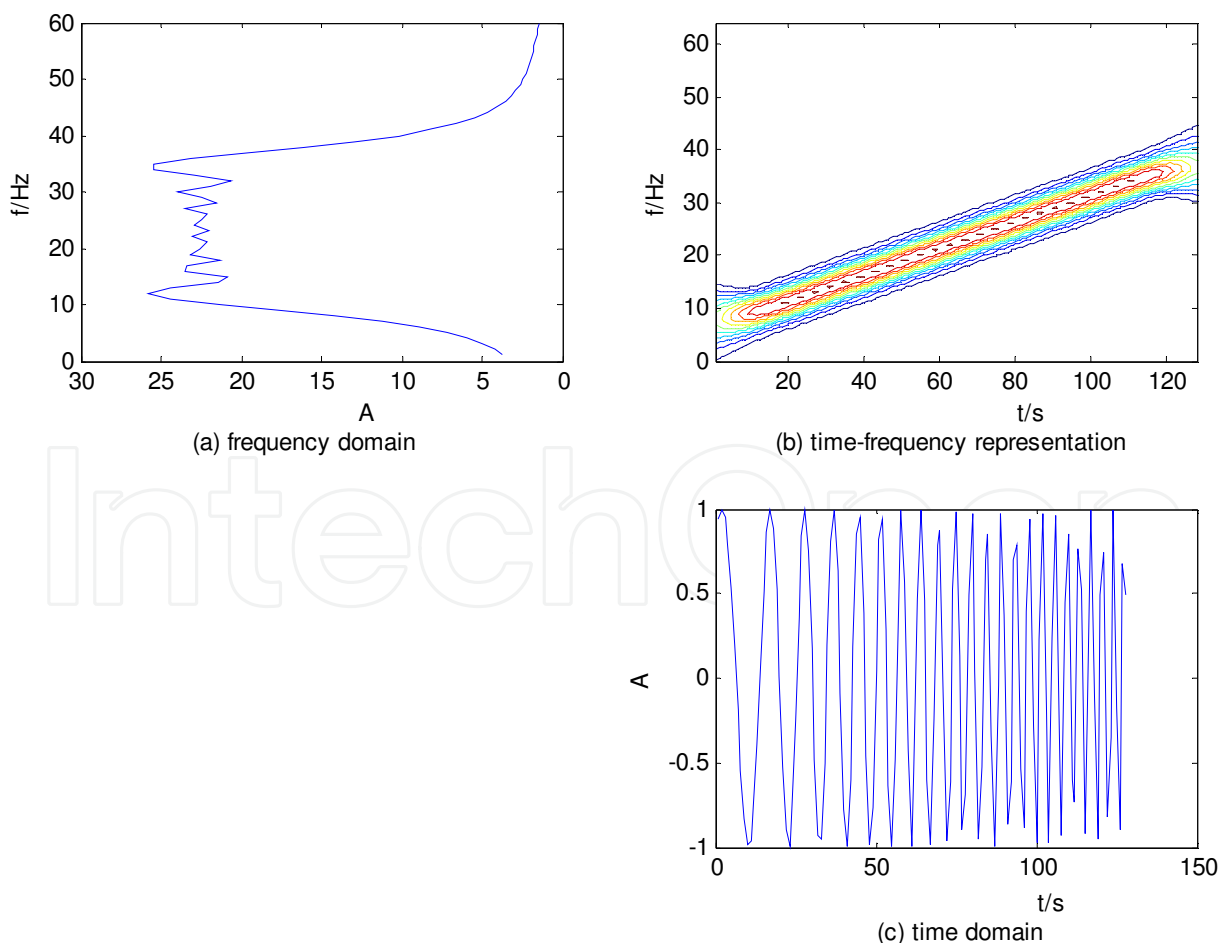


Fig. 5. Three description methods of linear frequency modulation signal

The basic idea of time-frequency analysis is to develop a joint function to combine the time and frequency factors. The time-frequency analysis, which can describe the signal traits on a time-frequency plane, has become an important research field. Many time-frequency methods have been presented, which can be divided into three types: linear, quadratic and nonlinear. The STFT and WT belong to the linear type, and the Wigner-Ville distribution (WVD) and pseudo Wigner-Ville distribution (PWVD) belong to the quadratic type. This section compares the STFT, WVD, PWVD and WT for showing the advantage of WT.

The basic idea of STFT, which is presented by Gabor in 1946, is to cut out the signal by a window function, in which the signal can be regarded as stationary, and analyze the signal to make sure the frequency elements in the window by the Fourier Transform, then move the window function along the time axis to obtain the change relationship of frequency over time. This is the time-frequency analysis process of STFT and the STFT of the signal  $x(t)$  can be described as:

$$\text{STFT}_x(t, f) = \int x(t') g^*(t' - t) e^{-j2\pi f t'} dt' \quad (13)$$

The WVD, which was presented by Wigner in the research of quantum mechanics in 1932 and applied to signal processing by Ville later, satisfies many mathematical properties expected by time-frequency analysis. The WVD of the signal  $x(t)$  can be described as:

$$\text{WD}_x(t, f) = \int x(t + \tau/2) x^*(t - \tau/2) e^{-j2\pi f \tau} d\tau \quad (14)$$

To suppress the disturbing of cross term in the WVD, the PWVD, which can be equivalent to smooth the WVD, is introduced. The PWVD of the signal  $x(t)$  can be described as:

$$\text{PWVD}_x(t, f) = \int h(\tau) x(t + \tau/2) x^*(t - \tau/2) e^{-j2\pi f \tau} d\tau \quad (15)$$

A nonstationary signal is analyzed in four time-frequency methods, i.e., STFT, WVD, PWVD and WT. Fig. 6 shows the oscillogram of a signal containing four Gauss components. The four time-frequency analysis results are shown in Fig. 7, in which (a), (b), (c) and (d) denote the results of STFT, WVD, PWVD and WT respectively. As shown in Fig. 7 (a), the resolution of STFT is lower and fixed. Although the WVD and PWVD have higher resolution and time-frequency concentration, they are disturbed strictly by cross terms as shown in Figs. 7 (b) and (c). In contrast, the resolution of WT is higher than STFT and can change with frequency. There is a good frequency resolution in the low frequency range, and a good time resolution in the high frequency range. And the cross terms in WVD and PWVD disappear. Though the STFT covers the shortage of the FT to some extent in local analysis, its defects cannot be overcome. That is, when the window function is determined, the size of windows is fixed and the time resolution and frequency resolution is fixed. As the resolution of window function is restricted by Heisenberg uncertainty principle, the frequency resolution is higher and the time resolution is lower when a long window is used, the situation is reversed when a short window is used. Therefore, the key of application is how to choose reasonable window length. When the signal which contains a variety of difference of scales is analyzed, the method of STFT becomes useless.

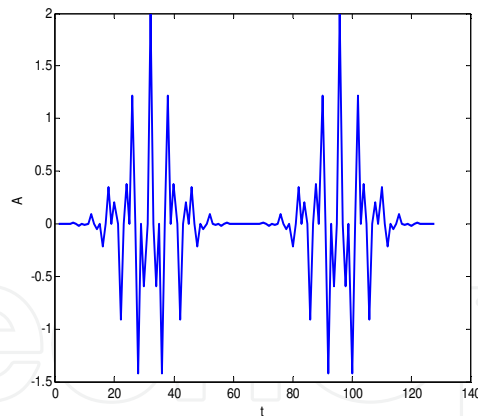


Fig. 6. The oscillogram of a signal contain four Gauss components

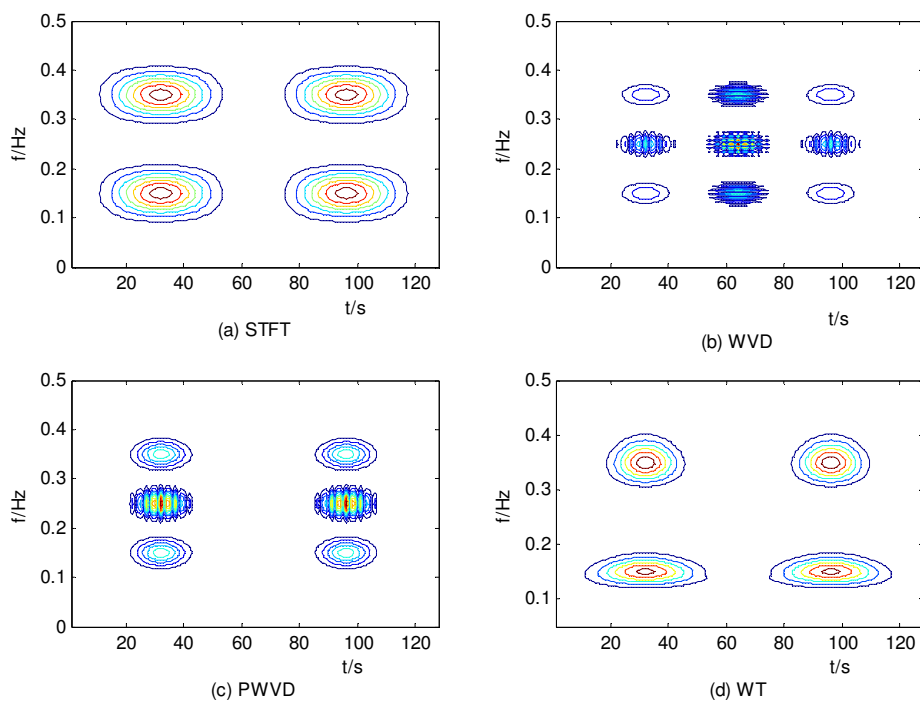


Fig. 7. Four time-frequency representations

The WVD has higher time-frequency resolution and many mathematical properties such as time-frequency concentration, symmetry, reversibility and normalizing. But the shortage is that it can not ensure non-negative and produce strictly cross terms especially for nonlinear signals, thus many researchers presented a variety of new patterns such as PWVD. These methods can suppress the disturbing signal of cross term to a certain extent, but they can not eliminate completely and damage many mathematical properties in WVD.

Although the WT is also restricted by Heisenberg uncertainty principle, the window in WT can be adjusted. In the WT, the mother wavelet can be stretched according to frequency to provide reasonable window, a long time window is used in low frequency and a short time window is used in high frequency. This time-frequency analysis which fully reflects the thought of multiresolution analysis is in accordance with the features of time varying nonstationary signal. Though the resolution of WT is lower than WVD and PWVD, the cross terms don't appear as the WT is linear time-frequency analysis.

### 4. Applications of the WT on nonstationary signals

This section gives some examples of the DWT successfully applied to nonstationary vehicle vibration and sound signals (Wang, et al, 2004, 2007, 2009, 2010).

#### 4.1 Wavelet transform for nonstationary vehicle vibration

Most of the research on vehicle vibration systems assumed that the vehicles were running at certain constant speeds, therefore, were regarded as a stationary random process. In more usual cases such as starting, accelerating and braking, vehicles work under variable speed conditions, and its vibration should be considered as a nonstationary process accordingly. For nonstationary signals, both the frequencies and their magnitudes vary with time, thus the conventional Fast Fourier Transform is incapable for dealing with them. The CWT and DWT were used to study the nonstationary inputs and responses of the vehicle vibration system (Wang and Lee, 2004).

A dynamic model of a full vehicle with eight degrees of freedom, was built shown in Fig. 8. And the corresponding differential equations were derived from the Lagrange equation as,

$$[M]\{\ddot{Z}\} + [C]\{\dot{Z}\} + [K]\{Z\} = [P]\{I(t)\} \tag{16}$$

Where  $[M], [C], [K]$  are matrixes of mass, damping and stiffness respectively,  $\{I(t)\}$  is the road roughness vector;  $[P]$  is the transfer matrix from the road roughness vector to the force excitation.  $\{z\}$  is the system response vector.

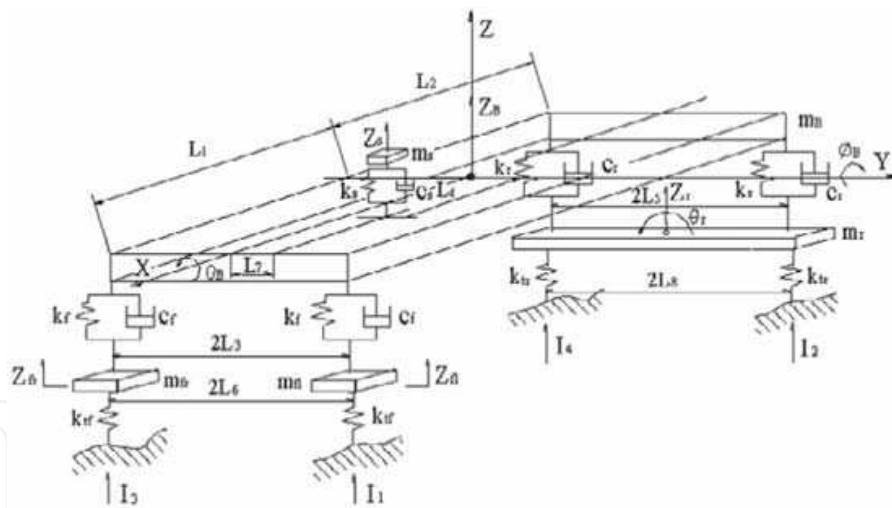


Fig. 8. Dynamic model of a vehicle with 8 DOFs

Assuming that the vehicle starting at a speed  $v_0 = 0$ , first accelerating with an acceleration  $a_1$  up to  $v_m$ , and then braking with a deceleration  $a_2$  down to  $v_f$ , the instantaneous vehicle speed at any time  $t$  were shown as,

$$V(t) = \begin{cases} v_0 + a_1 t & 0 < t < v_m / a_1 \\ v_m + a_2 (t - v_m / a_1) & v_m / a_1 < t < (v_m / a_1 + v_m / a_2) \end{cases} \tag{17}$$

The above process was called “AAB” process. Using the Runge-Kutta Method, the time series of road roughness and vehicle response were calculated by Eqs. (16) and (17).

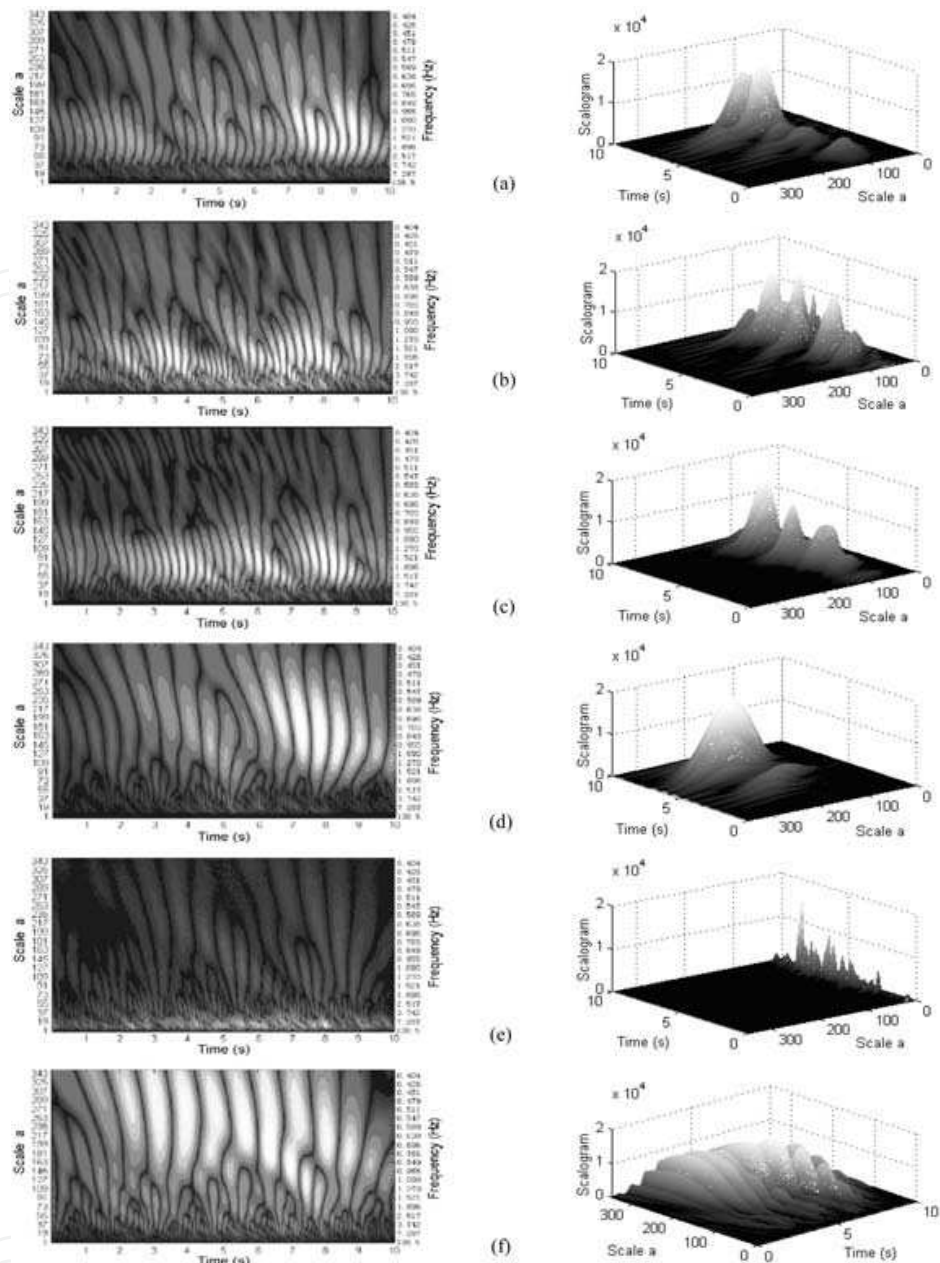


Fig. 9. 2D and 3D scalograms result from CWT during the “AAB” process: (a) the vertical vibration of the driver seat; (b), (c) and (d) the vertical, pitch and roll vibrations of the vehicle body; (e) the vertical vibration of the front axle; (f) the road roughness of the right-rear wheel.

The CWT and DWT are performed by using the Mallat algorithm in the Matlab toolbox. The selected parameters for calculation are: the Daubechies wavelet with a filter length of seven, the scaling factor  $a=1-350$ , i.e., the frequency range: 0.404-138.5 Hz. Fig. 9 (a)-(f) shows the acceleration scalograms, which were obtained from the CWT, of the seat, vehicle body, axle and road roughness during the “AAB” process, respectively. As seen from Fig. 9, the worst ride performance of the vehicle happened at 8s during the “AAB”, and there was a little time delay in the vibrations transfer from road to the vehicle system. In the accelerating process, the vibration energies of the vehicle are getting bigger, moving, as well, to the

higher-frequency area; their frequency bands are getting broader, and vice versa in the braking process. As a rule, these phenomena of energy flow are transmitted to the other levels through the suspension system.

In view of the vehicle design, the ride comfort of the passenger seat is the most important. Comparing Fig. 9 (a)-(f), the energy of road excitation has been greatly restrained by the suspension system of the vehicle. However, the similar time frequency traits can be seen in (a), (b) and (c), and the ride comfort of the seat deteriorates suddenly at a certain running speed. That means that the vertical and the pitching movement of the vehicle body have more effect on the vibration of seats than the rolling movement, and that the vibration energy of the vehicle body flowed into the resonance frequency region of the seat vibration system during the "AAB" process.

From the above findings, the WT can provide the time-frequency map of transient "energy flow" of the examined points of interest in the vehicle vibration system. Thus, the WT may be used in vehicle vibration system design, especially for the transient working cases.

#### 4.2 DWT-based denoising for nonstationary sound signals

In sound quality evaluation (SQE) engineering, distortion of the measured sounds by certain additive noises occurred inevitably, which came from both ambient background noise and the hardware of the measurement system; therefore, the signal needed to be denoised. In the former researches, we found that the unwanted noises are mainly white random noises which distributed in a wide frequency band but with small amplitudes. Some techniques for white noise suppression in common use, such as the least square, spectral subtraction, matching pursuit methods, and the wavelet threshold method have been used successfully in various applications. The wavelet threshold method in particular has proved very powerful in the denoising of a nonstationary signal. Here a DWT-based shrinkage denoising technique was applied for SQE of vehicle interior noise.

Sample vehicle interior noises were prepared using the binaural recording technique. The following data acquisition parameters were used: signal length, 10 s, sampling rate, 22 050 Hz. The measured sounds have been distorted by the random white random noises, and then wavelet threshold method is applied. This technique may be performed in three steps: (a) decomposition of the signal, (b) determination of threshold and nonlinear shrinking of the coefficients, and (c) reconstruction of the signal. Mathematically, the soft threshold signal is  $\text{sign}(x) (|x| - t)$  if  $|x| > t$ , and otherwise is 0, where  $t$  denotes the threshold. The selected parameters were: Daubechies wavelet "db3", 7 levels, soft universal threshold equal to the root square of  $2 \log(\text{length}(f))$ . As an example, a denoised interior signal and corresponding spectrum are shown in Fig. 10. It can be seen that the harmony and white noise components of the sample interior noise are well-controlled. The wavelet shrinkage denoising technique is effective and sufficient for denoising vehicle noises.

Based on the denoised signals, the SQE for vehicle interior noise was performed by the wavelet-based neural-network (WT-NN) model which will be mentioned in detail in the next section, the overall schematic presentation of the WT-NN model is shown in Fig. 11. After the model was well trained, the signals were fed to the trained WT-NN model and the Zwicker loudness model which is as reference. It can be seen that the predicted specific loudness and sharpness in Fig.12 are consistent with those from the Zwicker models. The wavelet threshold method can effectively suppress the white noises in the nonstationary sound signal.

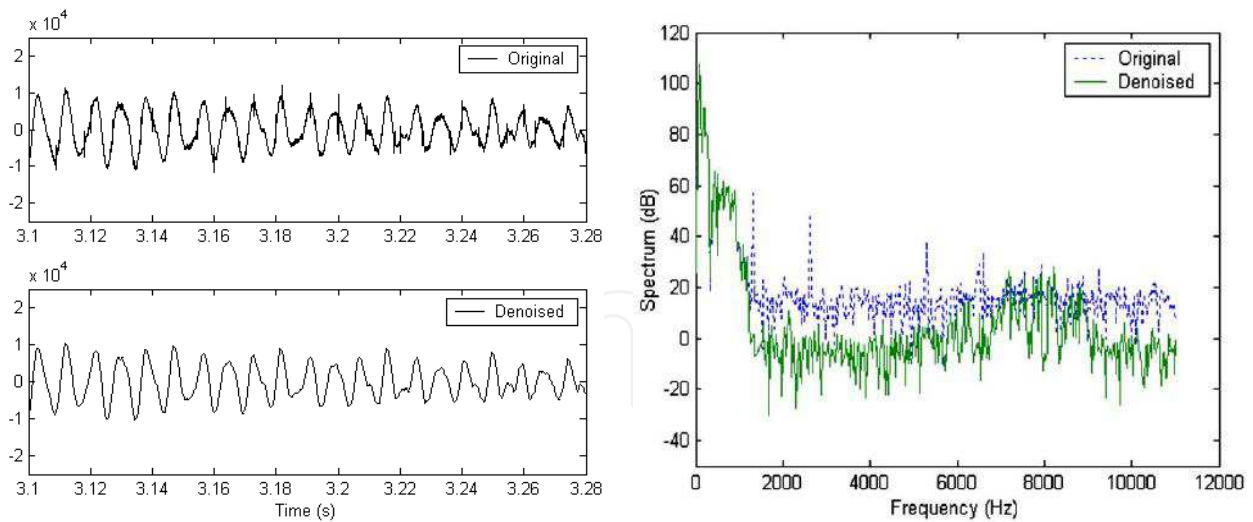


Fig. 10. Comparison of the interior noises (left panel) and their spectra (right panel) before and after the wavelet denoising model.

### 4.3 DWT for nonstationary sound feature extraction

In the above section, we mentioned a new model called WT-NN used for SQE for vehicle interior noise shown in Fig. 11. A wavelet-based, 21-point model was used as the pre-processor of the new WT-NN SQE model for extracting the feature of the nonstationary vehicle interior noise. For interpreting this new proposed model in detail, here we extend this model to another kind of noise-passing vehicle noise.

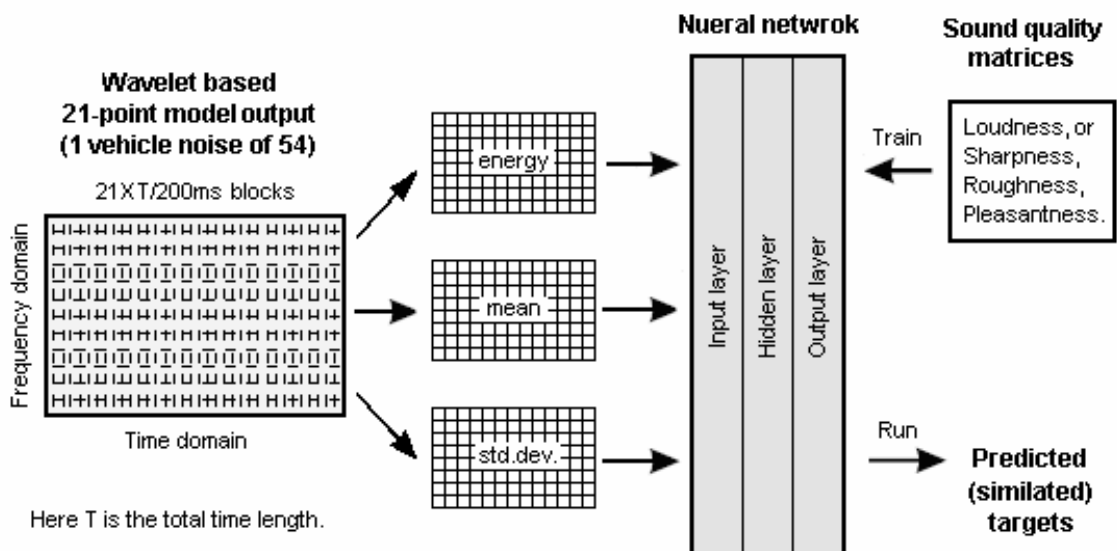


Fig. 11. Schematic presentation of the data inputs and outputs to the neural network

Sample passing vehicle noises were prepared identically as the above vehicle interior noises. The measured signals were denoised by using the wavelet threshold method mentioned before. Based on the pass-by vehicle noises, the 21-point feature extraction model for pass-by noises was designed by combining the a five-level DWT and a four-level WPA shown in Fig.13. It was used to extract features of the pass-by noises. The results are shown in Fig. 14.

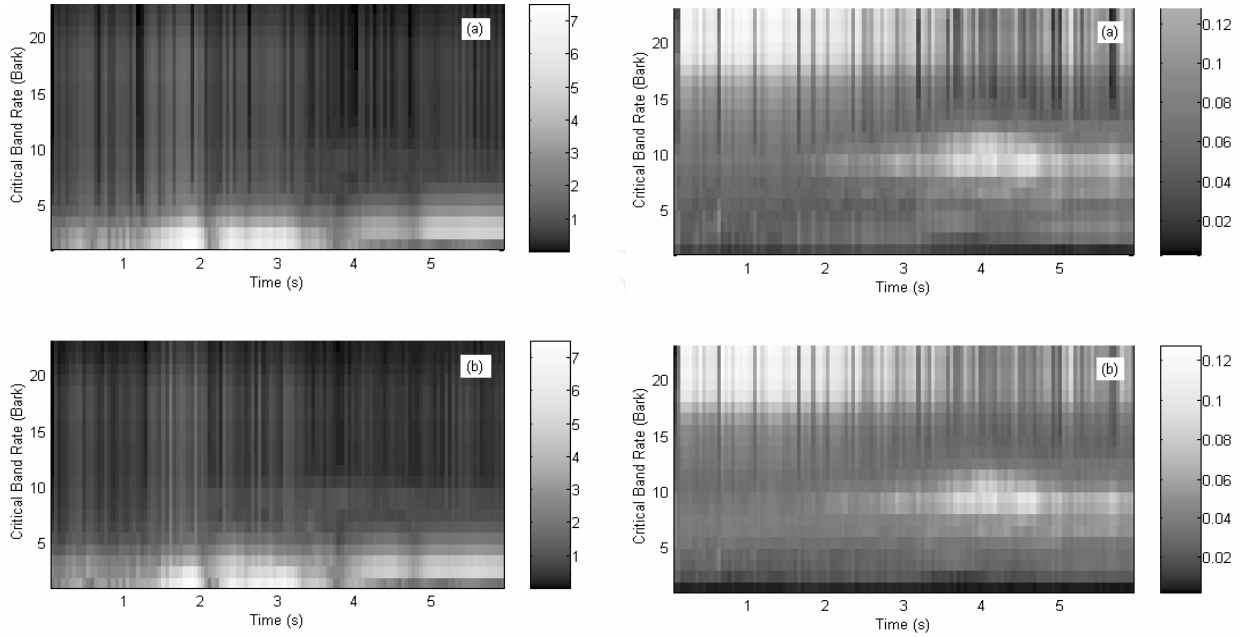


Fig. 12. Comparisons of specific loudness (left panel) and sharpness (right panel) between (a) the Zwicker model (upper), and (b) the WT-NN model (down)

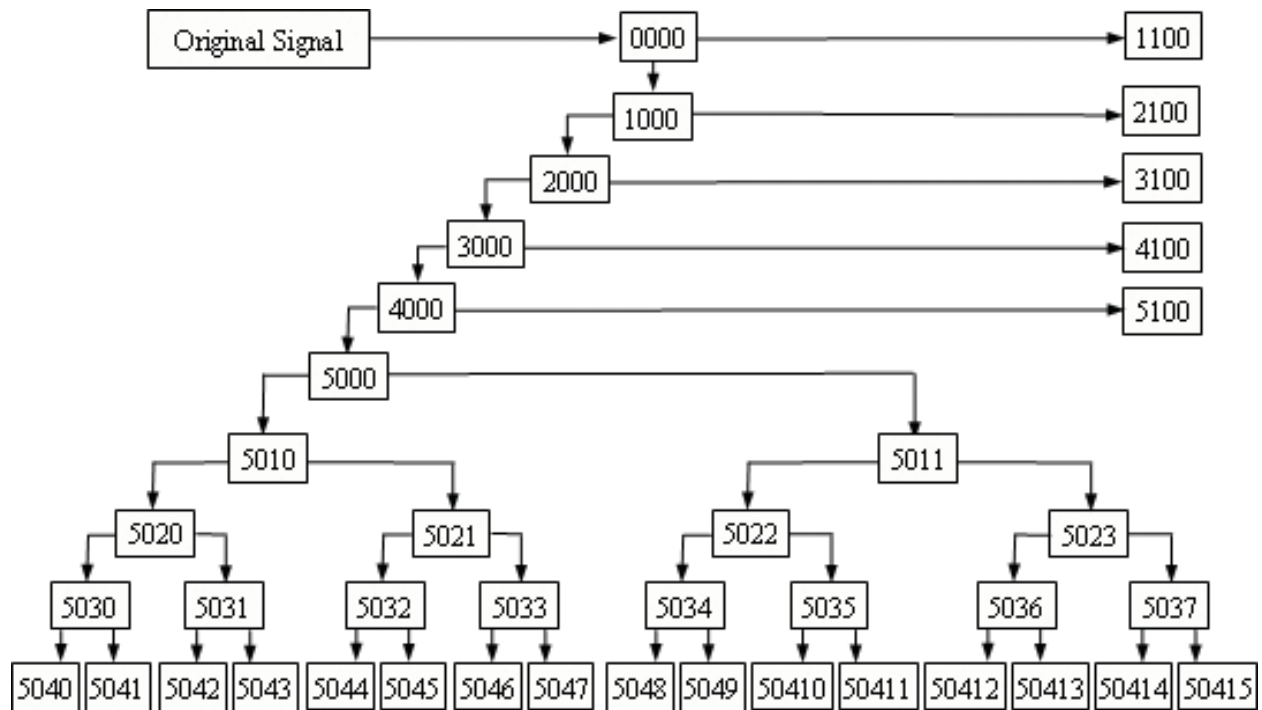


Fig. 13. Twenty-one-point wavelet-based feature extraction model for pass-by noise analysis

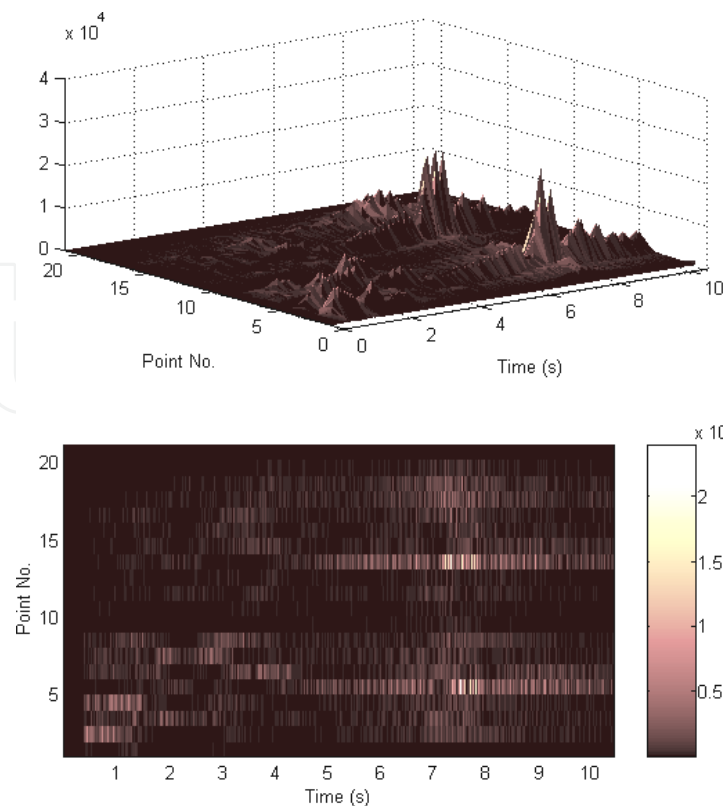


Fig. 14. Feature of the pass-by noise in time-frequency map extracted by the 21-point model

As the inputs of the WT-NN models, the above wavelet analysis results provide the time-frequency features of the signals. The SQM (sound equality matrices) of the pass-by noise as the outputs is taken from the psychoacoustical model. The loudness was adopted, which is related to the SQE of the vehicle pass-by noises. The output SQM is expressed as,

$$\text{SQM} = [\text{TL} \quad \text{SL}]^T$$

where the vectors TL and SL denote the total and specific values of loudness, respectively. After training the WT-NN model, the signals were fed into the Zwicker loudness model and the trained WT-NN model. It can be seen that the predicted specific loudness in Fig. 15 coincide well with those from the Zwicker models, thus as the pre-processor of the WT-NN model, the newly proposed wavelet-based, 21-point model can extract the feature of nonstationary signal precisely.

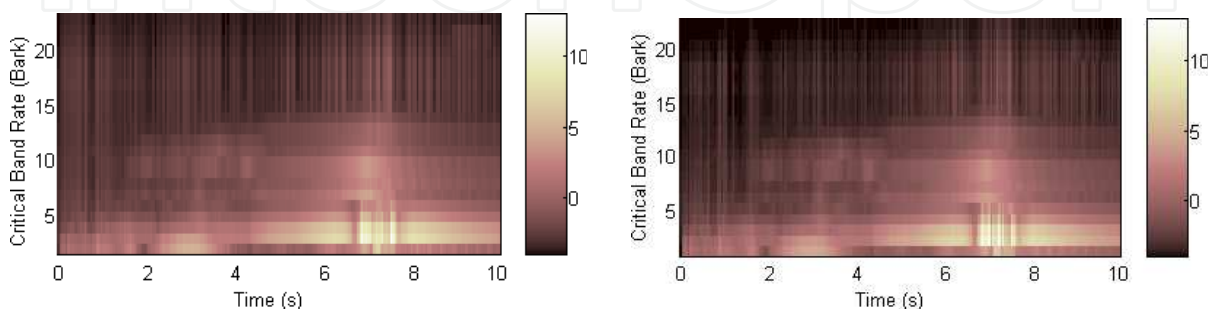


Fig. 15. Specific loudness comparison between (left panel) the Zwicker model, and (right panel) the WT-NN model.

#### 4.4 DWT for nonstationary sound quality evaluation

In this section a DWT-based filter bank is performed for sound octave band analysis (OBA). Verification results show that the DWT-based method (DWT-OBA) is accurate and effective for SQE of nonstationary vehicle noises.

In the measurements, a sample vehicle is accelerated up to a running speed 50 km/h. The following parameters for data acquisition are used: signal length, five seconds, sampling rate, 50 kHz. The measured sound signals need to be denoised for avoiding signal distortion by using the wavelet threshold method. Based on the measured interior vehicle noise, a DWT-OBA procedure is performed here. The determined wavelet function is the Daubechies wavelet with filter length of 70, i.e., 'db35'. The sound DWT-OBA of the interior noise can be performed in three steps: (a) signal resampling, (b) DWT filtering, and (c) band SPL calculation. The calculation procedure for the DWT-OBA of a sound signal is shown in Fig. 16. Then, the octave-band SPL values can be calculated from the sub-band filtered signals using the definition of sound pressure level in time domain,

$$L_i = 10 \log \left( \frac{1}{m_i} \sum_{j=1}^{m_i} p_{ij}^2 / P_{ref} \right) \quad (18)$$

where  $L_i$  is the  $i$ th band SPL,  $m_i$  is the total points of the  $i$ th band signal,  $P_{ij}$  is the  $i$ th band sound pressure on the  $j$ th point, and  $P_{ref}$  is the reference sound pressure,  $P_{ref} = 20e-6$ . Comparing with the measured results, the errors of the band SPLs in Fig. 21 are within  $[-0.3, +0.2]$  dB, which are much less than the band error scope of  $\pm 1$  dB defined in the IEC 651 standard. The total SPL are also computed by Eq. (19),

$$L_T = 10 \log \left( \sum_i 10^{L_i} \right) \quad (19)$$

It is exact same as the measured value 83.7 dB. In view of the A-weighted total SPL, the measured value is 66.1 dB (A), and the calculated value is 66.2 dB(A). To prove transient characteristic of the DWT-OBA algorithm, furthermore, the time-varying A-weighted total SPLs of the interior vehicle noise are carried out by using the DWT-OBA and MF-OBA algorithms, respectively. MF-OBA is a self-designed multi-filter octave band analysis method also used for SQE and here is adopted as reference. The selected calculation parameters are: time frame length, 200 ms, frame amount, 25, and A-weightings,  $[-56.7 -39.4 -26.2 -16.1 -8.6 -3.2 0 1.2 1.0 -1.1]$  dB, for octave band number from one to 10. The results shown in Fig. 17 imply a very good transient characteristic of the DWT-OBA.

In order to examine the effectiveness of the presented DWT-OBA algorithm for more practical uses, we applied it and the self-designed filtering algorithm to the measured exterior vehicle noise, respectively. The exterior noise signal has been pre-processed following the DWT denoising procedure. The A-weighted band SPLs of the exterior vehicle noise calculated from the filtering and DWT algorithms, as well as the measurement results, are shown in Figs. 18 and 19. And the calculated results are summarized in Table 1.

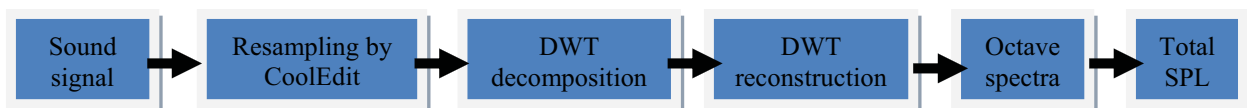


Fig. 16. The calculation flowchart for DWT octave-band analysis of a sound signal

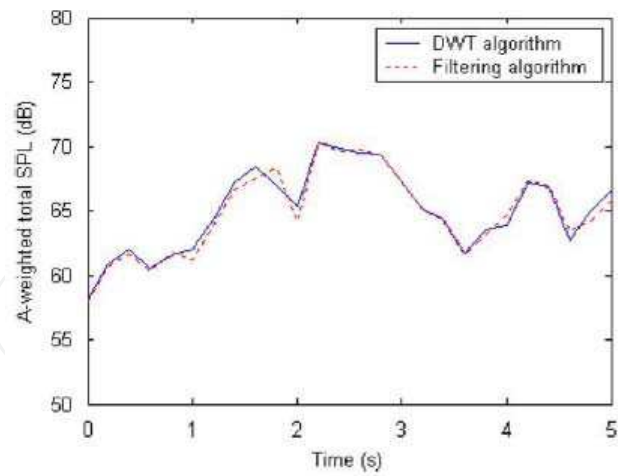


Fig. 17. Calculated time-varying A-weighted total SPLs of the interior vehicle noise by using the newly proposed DWT and filtering algorithms.

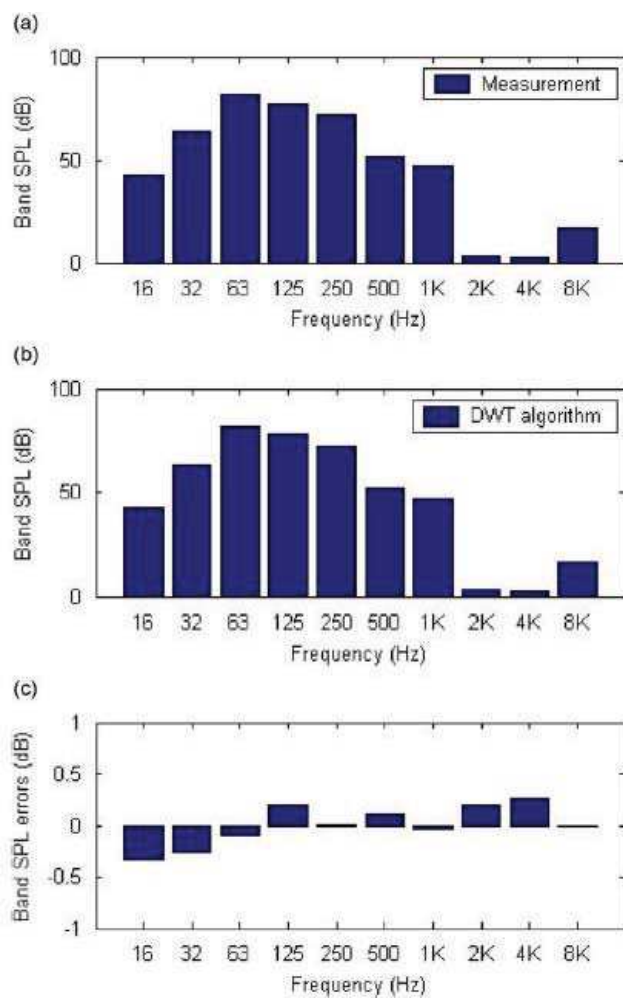


Fig. 18. Linear SPL comparison of the octave-band analysis of the interior vehicle noise: (a) the measured result, (b) SPL values calculated by the db35 filter bank, and (c) the band SPL errors

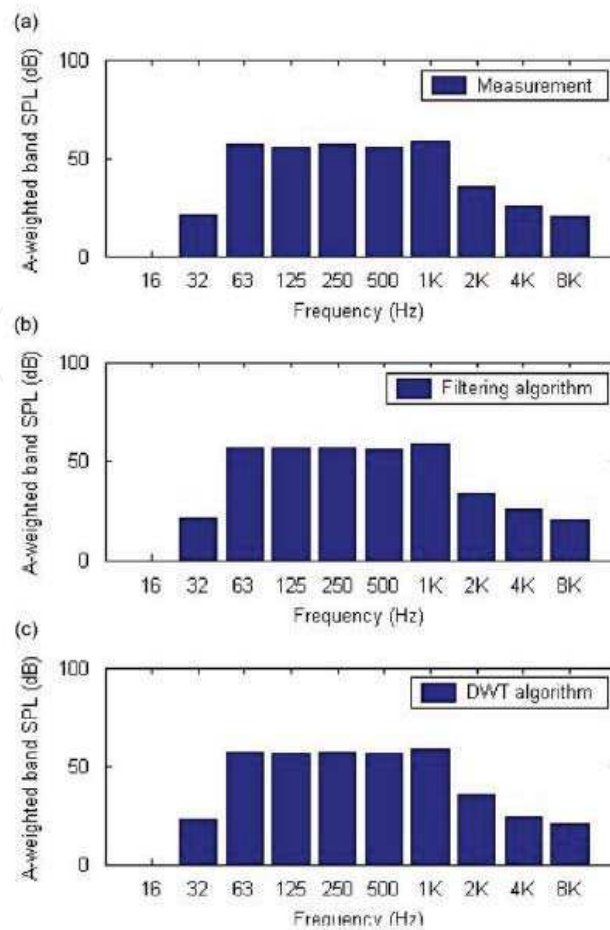


Fig. 19. A-weighted octave-band SPLs of the exterior vehicle noise from (a) the measurement, (b) self-designed filtering algorithm, and (c) the DWT algorithm.

Octave band number	1	2	3	4	5	6	7	8	9	10
Measured band SPLs(dB)	-13.2	21.0	56.8	55.9	56.7	55.9	58.8	35.4	25.5	20.2
Filtering band SPL error(dB)	-0.09	0.48	0.05	0.37	0.19	0.12	0	-0.07	0.27	0.17
DWT band SPL errors(dB)	-0.008	0.25	-0.08	0.24	0.09	0.18	0.04	0.02	0.03	-0.01
A-weighted total SPLs(dB)	64.0 (measured )				64.1476 (filtering)			64.0953 (DWT)		
Error percentage of total SPLs	0.2306% (filtering)				0.1489% (DWT)					

Table 1. Summary of the calculated A-weighted SPLs of the exterior vehicle noise from different methods

It can be seen that, for the exterior vehicle noise, the A-weighted SPLs from different methods have almost same octave patterns in frequency domain. From Table 1, the maximum errors of the filtering and DWT band SPLs are 0.48 and 0.25 dB, respectively,

which are all occurred in the octave band with a center frequency of 32 Hz. These errors can make very small contributions to the total SPL values, due to the special frequency characteristics of the vehicle noises. The octave band SPLs from the presented methods are satisfied the error limitation of  $\pm 1$  dB published in the IEC 651 standard. The error percentage of the A-weighted total SPLs are 0.2306% and 0.1489% for the filtering and DWT algorithms, respectively. The above comparisons indicate that the presented DWT-OBA algorithm is effective and feasible for sound quality estimation of vehicle noises.

#### 4.5 DWT pattern identification for engine fault diagnosis

In Section 4.2, 4.3 we proposed a new model called WT-NN in which the wavelet-based, 21-point feature extraction model was designed as the pre-processor. Here we performed this model for engine fault diagnosis (EFD), so called EFD WT-NN model.

To establish the EFD WT-NN model, firstly, a database including the engine fault phenomena and their corresponding sound intensity signals needs to be built. Based on the 2VQS type of EFI engine mounted on the GW-II engine test bed, the sound intensities in different failure conditions were measured using the two-microphone recording technique recommended by the standard ISO 9614. The experimental equipments are arranged as that in Fig. 20. The measured signals were denoised by using the wavelet threshold method.

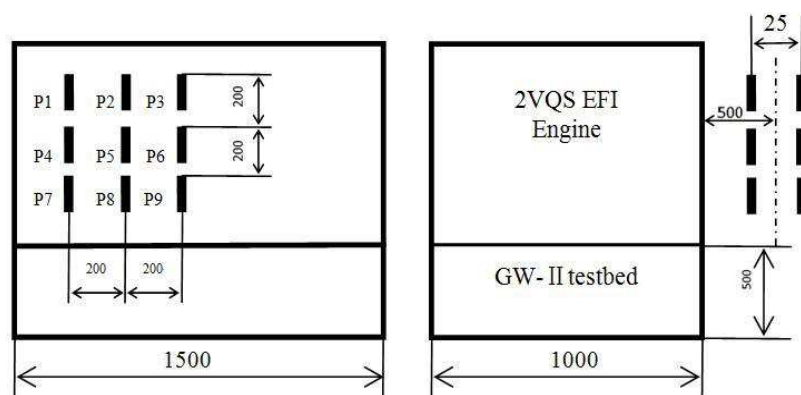


Fig. 20. Experimental setup for sound intensity measurements

To determine the structure of the time-frequency feature extraction model, the FFT-based spectral analysis is imposed on the above saved engine noise signals. The results suggest that the sound energies of the engine noises mainly distribute in a low-frequency range up to 3000 Hz (focus on the frequency interval [0-350Hz]), and decrease with increasing frequency. According to the above discussions, the wavelet-based, 21-point model for feature extraction of engine noises was applied. Using the 21-point model, the feature of the engine noises is extracted, and an example is shown in three dimensions in Fig. 21. Then the WT-NN model is built and performed for EFD. The noise signals in different engine state have been dealt with by applying the 21-point feature extraction model; the outputs of the pre-processor are defined in matrices and fed to a NN as the its inputs. Then, the failure phenomena corresponding to the engine state noise signals, which have been defined and quantified in matrices as shown in Table 2, are taken as the outputs of the NN.

After training, we respectively fed all the signals of different engine states to the trained WT-NN model. Typically, we listed the outputs of WT-NN model and the simulated diagnosis results (patterns) at the measuring point "P1" in Table 3, where the S0, S1, S2, ..., and S8, denoting the engine fault patterns have the same meanings as those in Table 2, and U is an uncertain result.

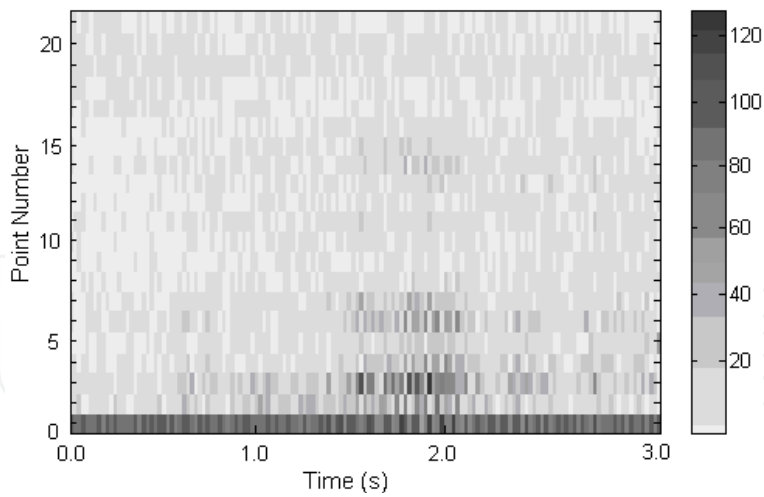


Fig. 21. The 21-point time-frequency feature of the engine fault state that the ECU does not receive the knock signals (meshing point no.2)

Engine working state	Target output
Normal idling state of the engine (S0)	[0 0 0 0 0 0 0 0]
The nozzle in the first cylinder doesn't work (S1)	[0 1 0 0 0 0 0 0]
The second and third cylinders do not work (S2)	[0 0 1 0 0 0 0 0]
The electric motor doesn't work (S3)	[0 0 0 1 0 0 0 0]
ECU does not receive the hall sensor signals (S4)	[0 0 0 0 1 0 0 0]
The throttle orientation potentiometer is broken (S5)	[0 0 0 0 0 1 0 0]
ECU does not receive the knock signals (S6)	[0 0 0 0 0 0 1 0]
The 5-voltage power of the hall sensor is broken (S7)	[0 0 0 0 0 0 0 1]
ECU does not receive the oxygen sensor signal (S8)	[0 0 0 0 0 0 0 1]

Table 2. The target output definition of the engine working states

Since the NN outputs are continuous values, the thresholds need to be defined to identify the calculated diagnosis results of the WT-NN model. Mathematically, the threshold rule is described as,

$$S_{fs} = \begin{cases} 0 & 0 \leq S_v \leq 0.45 \\ \text{uncertain} & 0.45 \leq S_v \leq 0.55 \\ 1 & 0.55 \leq S_v \leq 1.0 \end{cases}$$

where,  $S_{fs}$  denotes the fault state of the engine,  $S_v$  denotes the calculated output values of the WT-NN model. It can be seen that the diagnosis results in Table 4 is exactly same as that expected.

We obtained similar comparison results from the simulations using engine noise signals at other measuring points. We found that, for the sample signals used in the NN learning, the outputs of the BP network are in general conformity with the desired results; when the input data deviate from the samples within a certain range, the NN output has a tendency to approach the sample failure characteristics. For a real failure diagnosis, one may select in measurement points under the guidance of the NN designer of the diagnosis system. According to the above findings, the wavelet-based model may be used to diagnose engine failures in vehicle EFD engineering.

State	S0	S1	S2	S3	S4	S5	S6	S7	S8
Model output	0	0.164	0	0	0.027	0	0	0	0
	0	0.610	0	0	0.023	0	0	0	0
	0	0.022	0.989	0	0	0	0.009	0	0
	0.001	0	0	0.987	0.001	0	0.002	0.002	0
	0	0.016	0	0.034	0.970	0.002	0	0	0.085
	0.009	0	0	0.013	0	0.995	0.002	0.011	0
	0	0	0	0	0	0.001	0.979	0	0.088
	0	0	0	0.008	0	0	0	0.885	0
	0	0	0	0	0.023	0.004	0.030	0	0.976
Result	S0	S1	S2	S3	S4	S5	S6	S7	S8

Table 4. The outputs of the WT-NN model and diagnosis results at point "P1"

## 5. Acknowledgments

This work was supported by the NSFC (grant no. 51045007), and partly supported by the Program for Professor of Special Appointment (Eastern Scholar) at Shanghai Institutions of Higher Learning, China.

## 6. References

- Cohen, L. *Time-Frequency Analysis*. Prentice-Hall, New Jersey, USA, 1995.
- Brigham E. O., *The fast fourier transform and its applications*. Prentice-Hall, Englewood Cliffs, New Jersey, 1988
- Hodges C. H., Power J., Woodhouse J., The use of the sonogram in structure acoustics and an application to the vibrations of cylindrical shells, *Journal of Sound and Vibration*, 101, 203-218, 1985
- Baydar N., Ball A., A comparative study of acoustic and vibration signals in detection of gear failures using wigner-ville distribution. *Mechanical Systems and Signal Proceeding*, 15(6), 1091-1107, 2001
- Chen F. S., *Wavelet transform in signal processing theory and applications*. National Defense Publication of China, 1998
- Daubachies I., *Ten Lectures on Wavelets*, Philadelphia, PA: SIAM, 1992
- Wang Y. S., Lee C.-M., Zhang L. J., Wavelet Analysis of Vehicle Nonstationary Vibration Under Correlated Four-wheel Random Excitation, *International Journal of Automotive Technology*, Vol.5 No.4, 2004.
- Wang Y. S., Lee C.-M., Kim D.-G, Xu Y., Sound quality prediction for nonstationary vehicle interior noise based on wavelet pre-processing neural network model, *Journal of Sound and Vibration*, Vol 299, 933-947, 2007.
- Wang Y. S., Lee C.-M., Evaluation of nonstationary vehicle passing loudness based on an antinoise wavelet pre-processing neural network model, *Int. J. Wavelets, Multiresolution and Information Processing*, Vol 7, No.4, 459-480, 2009.
- Wang Y. S., Sound Quality Estimation for Nonstationary Vehicle Noises Based on Discrete Wavelet Transform, *Journal of Sound and Vibration*, Vol 324, 1124-1140, 2009.
- Wang Yansong, Xing Yanfeng, He Hui, An Intelligent Approach for Engine Fault Diagnosis Based on Wavelet Pre-processing Neural Network Model, *Proceedings of the 2010 IEEE International Conference on Information and Automation*, June 20-23, Harbin, China.



## **Discrete Wavelet Transforms - Theory and Applications**

Edited by Dr. Juuso T. Olkkonen

ISBN 978-953-307-185-5

Hard cover, 256 pages

**Publisher** InTech

**Published online** 04, April, 2011

**Published in print edition** April, 2011

Discrete wavelet transform (DWT) algorithms have become standard tools for discrete-time signal and image processing in several areas in research and industry. As DWT provides both frequency and location information of the analyzed signal, it is constantly used to solve and treat more and more advanced problems. The present book: Discrete Wavelet Transforms: Theory and Applications describes the latest progress in DWT analysis in non-stationary signal processing, multi-scale image enhancement as well as in biomedical and industrial applications. Each book chapter is a separate entity providing examples both the theory and applications. The book comprises of tutorial and advanced material. It is intended to be a reference text for graduate students and researchers to obtain in-depth knowledge in specific applications.

### **How to reference**

In order to correctly reference this scholarly work, feel free to copy and paste the following:

Yansong Wang, Weiwei Wu, Qiang Zhu and Gongqi Shen (2011). Discrete Wavelet Transform for Nonstationary Signal Processing, Discrete Wavelet Transforms - Theory and Applications, Dr. Juuso T. Olkkonen (Ed.), ISBN: 978-953-307-185-5, InTech, Available from: <http://www.intechopen.com/books/discrete-wavelet-transforms-theory-and-applications/discrete-wavelet-transform-for-nonstationary-signal-processing>

**INTECH**  
open science | open minds

### **InTech Europe**

University Campus STeP Ri  
Slavka Krautzeka 83/A  
51000 Rijeka, Croatia  
Phone: +385 (51) 770 447  
Fax: +385 (51) 686 166  
[www.intechopen.com](http://www.intechopen.com)

### **InTech China**

Unit 405, Office Block, Hotel Equatorial Shanghai  
No.65, Yan An Road (West), Shanghai, 200040, China  
中国上海市延安西路65号上海国际贵都大饭店办公楼405单元  
Phone: +86-21-62489820  
Fax: +86-21-62489821

© 2011 The Author(s). Licensee IntechOpen. This chapter is distributed under the terms of the [Creative Commons Attribution-NonCommercial-ShareAlike-3.0 License](https://creativecommons.org/licenses/by-nc-sa/3.0/), which permits use, distribution and reproduction for non-commercial purposes, provided the original is properly cited and derivative works building on this content are distributed under the same license.

IntechOpen

IntechOpen